Accelerated variational approach for searching cycles

Ding Wang,[1] Peijie Wang,[1,*] and Yueheng Lan[2,3,†]
[1]*The Beijing Key Laboratory for Nano-Photonics and Nano-Structure, Department of Physics, Capital Normal University, Beijing 100048, China*
[2]*State Key Lab of Information Photonics and Optical Communications, Beijing University of Posts and Telecommunications, Beijing 100876, China*
[3]*School of Science, Beijing University of Posts and Telecommunications, Beijing 100876, China*

(Received 24 May 2018; revised manuscript received 3 September 2018; published 2 October 2018)

Several schemes are proposed to accelerate the recently designed variational approach for finding periodic orbits in a nonlinear system with chaotic dynamics, especially those close to a singularity or with long period. An effective equation is derived to implement an automatic allocation of lattice points to capture local fine orbit structures while keeping the exponential convergence of the variational approach. Utilizing the special structure of the matrix involved in the homotopy evolution, the lower–upper (LU) decomposition could be done with much greater efficiency and much less memory, which considerably facilitates the search for long cycles. Three examples are used to demonstrate the validity of the accelerated algorithm. For Hamiltonian systems, an interesting scheme is designed to remove the neutral direction associated with the conservation law while keeping the dynamics on the desired energy surface.

DOI: 10.1103/PhysRevE.98.042204

I. INTRODUCTION

In a Hamiltonian system, the dynamics becomes increasingly chaotic when its parameters move away from those in the integrable regime. Although invariant tori gradually get destroyed in this process [1–3], many periodic orbits survive or are created and serve as the skeleton of the asymptotic dynamics. In general, periodic orbits could be conveniently used to study the long-term behavior of a nonlinear system [1], for which cycle expansions are very efficient in computing average values of physical observables [4–6] on the strange attractors, where cycles are ordered hierarchically in terms of their topological length or stability. Even in the microscopic world governed by quantum mechanics, cycles could still be utilized to carry out the semiclassical computation. For example, in a molecular system [7], although most trajectories are chaotic, periodic orbits could still be effectively used for the quantization of a system. With quite high accuracy, different energy levels or state densities are accessible in terms of averages on short periodic orbits. Therefore, it is of great significance to locate periodic trajectories, especially short ones for the study of dynamical properties of a nonlinear system.

Over past several decades, many methods have been proposed to search for periodic orbits [8–15], such as the Newton-Raphson method or its variants [15,16], which are applicable to a large variety of dynamical systems. But, for a long periodic orbit, it requires a very good initial guess that is close to a true cycle. Even still, the method is likely to fail in high-dimensional systems [17,18]. To reduce the cumulative error in the long-time evolution, in the multiple shooting scheme, a set of Poincaré sections in the phase space is selected to divide the cycle into short pieces. However, it is hard to locate these many sections in the phase space of a nonlinear system with complex dynamics, especially in a high-dimensional system. This difficulty is subdued in a variational approach proposed in Ref. [10], which eliminates most Poincaré sections by discretizing continuous time evolution into small time steps. Specifically, a guess loop is put in the phase space rather than a single point, which is driven to a desired true orbit exponentially fast by a fictitious time flow. The computation is highly stable and successfully applied even to high-dimensional systems.

Nevertheless, the variational approach requires storage of an entire trajectory in the computer memory, which is heavy, especially for high-dimensional dynamical systems. Furthermore, the computation load is at least proportional to the number of discretization points, which may significantly slow the computation. In an effort of extending the method to search for connecting orbits [19], an automatic mesh allocation algorithm is designed to make the guess points evenly distributed in arc length instead of in time to avoid their cumulation near the two ends of the connection where the flow is exponentially approaching zero. It works nicely for searching orbits connecting two equilibria. However, complications may arise in search for an orbit of more general type, e.g., a periodic orbit. Around a fixed point or a singularity, the orbit structure may get intricate, or even worse, the dynamics could turn nearly singular, which may fail the variational approach in resolving the detailed structures at fine space or time scales. In this case, an improved version is in need to ensure both the efficiency and accuracy.

In the current work, in order to find such a "pathological" cycle, we use different schemes to allocate mesh points in different situations, which greatly reduces the number of required lattice points with reasonable accuracy being kept

*Corresponding author: pjwang@cnu.edu.cn
†Corresponding author: lanyh@bupt.edu.cn

[19–21]. Meanwhile, the program becomes more robust even when a true singularity is approached since the intricate dynamics or orbit structure could be much better resolved with properly distributed lattice points. To get a better guess, the homotopy evolution is often invoked: start with a periodic orbit away from the singularity, and then homotopically evolve the orbit to the critical point by gradually changing the system parameters. The variational approach is born for this type of evolution and is thus very efficient. As before, the adaptive time step is used in the calculation based on the smoothness of the evolution. These improvements pave the way for application of the variational method in many near-singular cases.

The paper is organized as follows. In Sec. II, the variational equation is modified to automatically allocate lattice points according to a given rule but still keep the exponential convergence. In Sec. III, the lower–upper (LU) decomposition is optimized based on the special structure of the evolution matrix and an interesting algorithm is proposed to remove the singularity associated with the conservation law. In Sec. IV, three examples are used to demonstrate the validity of the improved variational approach. We summarize the paper and point to possible future applications in Sec. V.

II. THE VARIATIONAL METHOD WITH AUTOMATIC ALLOCATION OF LATTICE POINTS

We consider a general dynamical system which is defined by a set of ordinary differential equations (ODEs):

$$\frac{d}{dt}x(t) = \boldsymbol{v}(\boldsymbol{x}(t)), \tag{1}$$

where $x \in R^d$, $t \in R$, and $v(x)$ is a smooth function defined in the phase space. If there is a trajectory $x(t)$ of Eq. (1) that satisfies the condition

$$f^T(\boldsymbol{x}) = \boldsymbol{x}, \tag{2}$$

where $f^t(\boldsymbol{x})$ indicates the evolution result of x under system dynamics (1) in a time interval t and $T > 0$ is the smallest positive number that satisfies this condition, we refer to this type of trajectory as a periodic orbit and T is the period. Quite many methods for finding periodic orbits have been designed and applied [10–12,22,23] in recent years. Nevertheless, for high-dimensional or complex systems, such as the Kuramoto-Sivashinsky system in a spatiotemporally turbulent regime, the variational approach shows great robustness and versatility [10].

We recall first the variational method previously designed for the determination of periodic orbits in Eq. (1) (see Refs. [10] and [24]), which drives a loop in the phase space to a true cycle by a fictitious evolution equation,

$$\frac{\partial^2\tilde{x}}{\partial s\partial\tau} - \lambda\frac{\partial v}{\partial x}\frac{\partial\tilde{x}}{\partial\tau} - v\frac{\partial\lambda}{\partial\tau} = \lambda v - \frac{\partial\tilde{x}}{\partial s}, \tag{3}$$

where $\tilde{v} = \frac{\partial\tilde{x}}{\partial s}$ ($\tilde{x} \in R^d$) is the loop velocity, $\tilde{x}(\tilde{x} \in R^d)$ marks the representative points of the loop and is parameterized by $s(s \in [0, 2\pi])$, τ is the fictitious time which records the evolution from an initial guess loop to the desired periodic orbit, and v is the velocity field of the dynamical systems along the guess loop given in Eq. (1). The parameter λ is a constant which is used to match the magnitude of v and $\tilde{v}$, or in other words, to adjust the period. We may rewrite Eq. (3) in a more concise form as follows:

$$\frac{\partial}{\partial\tau}(\tilde{v} - \lambda v) = -(\tilde{v} - \lambda v), \tag{4}$$

which could be formally solved

$$\tilde{v} - \lambda v = e^{-\tau}(\tilde{v} - \lambda v)|_{\tau=0}\,, \tag{5}$$

showing that the value of $\tilde{v} - \lambda v$ converges exponentially with the increase of τ as the loop continuously evolves toward the periodic orbit. However, if there is a nonzero local minimum for the squared deviation $(\tilde{v} - \lambda v)^2$, the evolution of Eq. (3) will become singular and lead to blowup. Usually, a good initial guess may avoid this trouble. Nevertheless, if there are too few lattice points, the cycle could not be represented authentically; it is impossible to reduce the error to a sufficiently small value which may fail the program as well. This happens quite often near a singularity where the orbit structure becomes finely twisted with dynamics varying violently. As a result, for a uniform in time distribution of the lattice points, in order to reduce the error, a large number of points are needed, which may choke the computer memory and tremendously slow the program.

In fact, the computation would become much more efficient if we only increase the lattice points near the singularities (or fixed points), keeping the points in other places more or less balanced. Based on this consideration, a moving mesh is introduced by reparametrizing periodic orbits to redistribute the lattice points in a way that caters to our need. In Eq. (3), the parameter s is supposedly proportional to the time along the trajectory, which may not be the best and should be replaced by a better scheme in the above-mentioned cases. Suppose that s could be reparametrized as $s = s(\alpha)$ by a new parameter α, $\alpha \in [0, 2\pi]$ so that

$$\frac{\partial}{\partial s} = \frac{d\alpha}{ds}\cdot\frac{\partial}{\partial\alpha}, \tag{6}$$

where $\frac{d\alpha}{ds} = \omega(x(s))$ is a weight function [20] which monitors the density of lattice points. If points are distributed uniformly in α, then in s or in time, the point density is proportional to $\omega(x(s))$. Therefore the choice of the weight function is essential. With this new parameter, Eq. (3) becomes

$$\omega\frac{\partial^2\tilde{x}}{\partial\alpha\partial\tau} - \left[\lambda\frac{\partial v}{\partial x} - \left(\frac{\partial\tilde{x}}{\partial\alpha}\right)\frac{\partial\omega}{\partial x}\right]\frac{\partial\tilde{x}}{\partial\tau} - v\frac{\partial\lambda}{\partial\tau} = \lambda v - \omega\frac{\partial\tilde{x}}{\partial\alpha}, \tag{7}$$

which still satisfies Eq. (4) and hence converges in the fictitious time if the definition $\tilde{v} = \frac{\partial\tilde{x}}{\partial\alpha}$ is used. Note that a new term appears in Eq. (7), which distinguishes Eq. (7) from the corresponding Eq. (10) in a previous paper [19].

In many applications [19,20], the weight function could be written as

$$\omega(t) = \sqrt{\gamma + c|\bar{\boldsymbol{v}}_t|^2}, \tag{8}$$

where γ and c are two adjusting parameters and γ could be set to 1. If $c = 0$, then ω is a constant which indicates that α

is proportional to s, and thus the lattice points distribute uniformly in time. When $C \to \infty$, $\omega(t) \sim |\mathbf{v}_t|$, α is parameterized by the arc length. Different distributions can be obtained by adjusting these parameters. When the cycle approaches a singularity where the coordinates change rapidly, the above parameterization might still not be valid and other types of choices are needed.

III. NUMERICAL IMPLEMENTATION

The periodic orbit is invariant if all the lattice points move along the trajectory for the same time interval. This translational invariance will supply a neutral direction to the update of the coordinates, which will undermine the solution of the fictitious time evolution [10]. In order to remove the translational invariance, a gauge-fixing condition is added [18,19,25], one form of which will be employed in the following. In a discretization of a loop, the velocity along the loop reads

$$\tilde{v}_n = \left.\frac{\partial \tilde{x}}{\partial s}\right|_{\tilde{x}=\tilde{x}_n} \approx (\hat{D}\tilde{x})_n. \tag{9}$$

With a five-point approximation scheme, $\hat{D}$ with the periodic condition is rewritten as

$$\hat{D} = \frac{1}{12h}\begin{pmatrix} 0 & 8 & -1 & & & & & & 1 & -8 \\ -8 & 0 & 8 & -1 & & & & & & 1 \\ 1 & -8 & 0 & 8 & -1 & & & & & \\ & & & & \vdots & \ddots & & & & \vdots \\ & & & & & 1 & -8 & 0 & 8 & -1 \\ 1 & & & & & & 1 & -8 & 0 & 8 \\ 8 & -1 & & & & & & & -8 & 0 \end{pmatrix}, \tag{10}$$

where $h = 2\pi/N$, and each entry represents a $d \times d$ matrix, with blank space filled with zeros. In our numerical work, along with the gauge-fixing condition, the discretized version of Eq. (7) with the choice $\omega(t) \sim |\bar{v}_t|$ can be written as

$$\begin{pmatrix} \hat{A} & -\hat{v} \\ \hat{a} & 0 \end{pmatrix}\begin{pmatrix} \delta\hat{x} \\ \delta\lambda \end{pmatrix} = \delta\tau \begin{pmatrix} \lambda\hat{v} - |\bar{v}_t|\widehat{\tilde{v}} \\ 0 \end{pmatrix}, \tag{11}$$

where

$$\hat{A} = |\bar{v}_t|\hat{D} - \mathrm{diag}[\lambda A_1 - B_1, \lambda A_2 - B_2, \ldots, \lambda A_N - B_N],$$

with $A_n = \frac{\partial v_i}{\partial x_j}$ (being the Jacobian matrix of the velocity field), and $B_n = (\frac{\partial \tilde{x}}{\partial \alpha})\frac{\partial |\bar{v}_t|}{\partial x}$ is a $d \times d$ matrix. $\widehat{\tilde{v}} = (\tilde{v}_1, \tilde{v}_2, \ldots, \tilde{v}_N)'$ and $\hat{v} = (v_1, v_2, \ldots, v_N)'$ respectively represent the loop velocity vector field and the velocity vector field of the flow which the loop goes through. $\hat{a}$ is an Nd-dimensional row vector representing the gauge-fixing condition,

$$\hat{a} \cdot \delta\mathbf{x} = 0,$$

which adds a linear constraint to the change of the coordinates. In the current situation, one specific choice would be $\hat{a} \to (1, 0, 0, \ldots, 0)$, which would fix just the first coordinate of the first point and limit the motion of the first point to a (d-1) dimensional hyperplane, while other representative points are rearranged by the weight function $\omega(t)$. By solving Eq. (11) repeatedly, the coordinates of the guess loop are updated step by step, so that the initial loop exponentially converges to the true periodic orbit which we want to find.

In order to reduce the memory load and accelerate the computation, in the previous section we designed an automatic mesh allocation scheme to reduce the number of lattice points for accurately characterizing a periodic orbit. Here, we may obtain another reduction of the computation load by a more efficient LU decomposition scheme. From the above analysis, we see that the inversion of the matrix equation (11) is the most time-consuming part in the evolution. However, in view of the special structure of the matrix involved, the LU decomposition [21] could be greatly simplified such that the computation load is proportional to the size Nd of the matrix instead of its square, thus enabling the search for long cycles and a more detailed characterization of chaotic dynamics. The matrix $\left(\begin{smallmatrix} \hat{A} & -\hat{v} \\ \hat{a} & 0 \end{smallmatrix}\right)$ on the left-hand side of Eq. (11) has a band diagonal form and as a result the L and U matrices could be written as follows:

$$\mathrm{L} = \begin{pmatrix} 1 & & & & & & & & & \\ a_0 & 1 & & & & & & & & \\ b_0 & a_1 & 1 & & & & & & & \\ & b_1 & a_2 & 1 & & & & & & \\ & & & \ddots & \ddots & \ddots & & & & \\ & & & & b_{N-5} & a_{N-4} & 1 & & & \\ c_0 & c_1 & c_2 & & c_{N-5} & c_{N-4} & c_{N-3} & 1 & & \\ d_0 & d_1 & d_2 & \cdots & d_{N-5} & d_{N-4} & d_{N-3} & d_{N-2} & 1 & \\ e_0 & e_1 & e_2 & & e_{N-5} & e_{N-4} & e_{N-3} & e_{N-2} & e_{N-1} & 1 \end{pmatrix}, \tag{12a}$$

$$\mathrm{U} = \begin{pmatrix} f_0 & g_0 & h_0 & & & & i_0 & j_0 & k_0 \\ & f_1 & g_1 & h_1 & & & i_0 & j_0 & k_0 \\ & & \ddots & \ddots & \ddots & & \vdots & \vdots & \vdots \\ & & & f_{N-5} & g_{N-5} & h_{N-5} & i_{N-5} & j_{N-5} & k_{N-5} \\ & & & & f_{N-4} & g_{N-4} & h_{N-4} & j_{N-4} & k_{N-4} \\ & & & & & f_{N-3} & g_{N-3} & h_{N-3} & k_{N-3} \\ & & & & & & f_{N-2} & g_{N-2} & k_{N-2} \\ & & & & & & & f_{N-1} & k_{N-1} \\ & & & & & & & & f_N \end{pmatrix}, \tag{12b}$$

where each element in the matrices given above is a $d \times d$ matrix. Both L and U have a tridiagonal form with three more rows (for L) or columns (for U) filled at the bottom or the right end. As usual, the matrix elements of L and U are determined by the identity

$$P_{ij} = \sum_{k=1}^{i-1} l_{ik} u_{kj}$$

in a straightforward way if proper care is exercised. In the present, however, the number of unknown elements in L and U is proportional to Nd instead of $(Nd)^2$ as in the usual LU decomposition, which greatly speeds up the computation, especially when the method is applied together with an adaptive step size scheme based on the smoothness of the fictitious evolution devised in Ref. [10]. When the loop is close to a periodic orbit, the step size can be set to the full Newton one $\delta\tau = 1$.

A conservation law in a dynamical system may supply a neutral direction for the variation of the lattice points and hence make Eq. (11) near singular. In a commonly seen Hamiltonian system, the energy is very likely to be conserved, which may set our searching program awry. Here we use a two-dimensional Hamiltonian as an example to present one possible way to remove this trouble. Suppose that the Hamiltonian is

$$H = H(\mathrm{x}, \mathrm{y}, p_x, p_y), \tag{13}$$

where x, y, p_x, p_y are four parameters describing the state of a system, and the equation of motion of the Hamiltonian system could be written as

$$\dot{x} = \frac{\partial H}{\partial P_x} \quad \dot{P}_x = -\frac{\partial H}{\partial x},$$
$$\dot{y} = \frac{\partial H}{\partial P_y} \quad \dot{P}_y = -\frac{\partial H}{\partial y}.$$

If we denote $\mathbf{X} = \begin{pmatrix} x \\ y \\ P_x \\ P_y \end{pmatrix}$, then the canonical equation could be written as

$$\dot{\mathbf{X}} = \begin{pmatrix} \dot{\mathbf{x}} \\ \dot{\mathbf{y}} \\ \dot{\mathbf{P}}_\mathbf{x} \\ \dot{\mathbf{P}}_\mathbf{y} \end{pmatrix} = M \cdot \nabla H \ \text{ with } \ M = \begin{pmatrix} 0 & 1 \\ -1 & 0 \end{pmatrix}, \tag{14}$$

where $\mathbf{1}$ is a 2×2 unit matrix, resulting in

$$\frac{d\boldsymbol{H}}{dt} = \nabla H \cdot \dot{\mathbf{X}} = 0. \tag{15}$$

Equation (15) is a mathematical expression of the energy conservation. If we concentrate on a specific energy level E_0, to remove the conservation law, we add one extra term to the original dynamics equation, so that

$$\dot{\mathbf{X}} = \boldsymbol{M} \cdot \nabla H + \beta \cdot (E_0 - H) \cdot \nabla \mathrm{H}, \tag{16}$$

where the second term on the right is zero at the desired energy surface E_0–$H = 0$. The equation of motion does not change at this energy. In addition, according to Eqs. (16) and (15), we have

$$\frac{d(H - E_0)}{dt} = \nabla(H - E_0) \cdot \dot{\mathbf{X}} = \beta \cdot (E_0 - H) \cdot (\nabla H)^2, \tag{17}$$

which drives a representative point back to the desired surface if it deviates from the prescribed energy. In this way, all previous formulas could still be used and a different energy surface is considered for different E_0 values.

IV. APPLICATIONS

In this section we show the validity of the modified variational method by applying it to several classical models. In all the computations, the convergence condition is

$$F = \sqrt{\sum_{i=1}^{N} (\tilde{v}_i - \lambda v_i)^2} \leqslant 10^{-6}. \tag{18}$$

A. Example 1

We first apply the modified method to the search of the periodic orbit in the Lorenz equation [26], which reads

$$\begin{aligned} \dot{x} &= \sigma(y - x) \\ \dot{y} &= x(\rho - z) - y \\ \dot{z} &= xy - \mu z. \end{aligned} \tag{19}$$

The origin is a fixed point for all parameter values and the z axis is invariant under the evolution (19). The system is invariant for $x \to -x$, $y \to -y$ so that a periodic orbit is either symmetric or has a symmetry partner. At $\sigma = 10$, $\mu = 8/3$, $\rho = 13.926\,56$, a homoclinic explosion [27] takes place where a pair of cycles are born with increasing ρ. However, if the value of ρ is close to 13.926 56, the cycle bears great resemblance to the mother homoclinic orbit and is nearly singular (shown in Fig. 1) close to the fixed point. As a result,

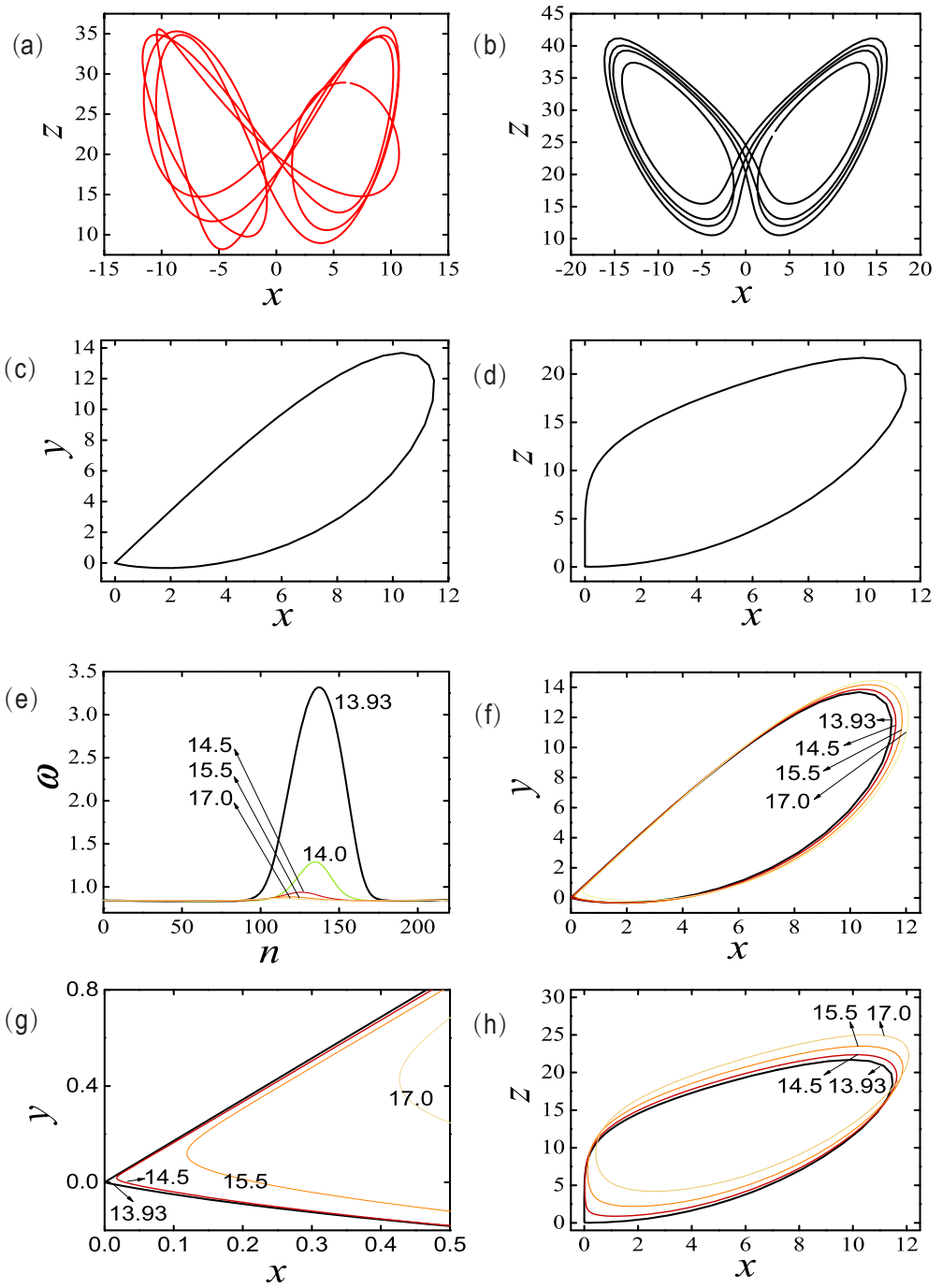

FIG. 1. (a), (b) The projections in the X-Z plane of the initial guess loop (red line) and the butterflylike periodic orbit obtained by our modified method at $\rho = 28$. (c), (d) The periodic orbit at $\rho = 13.93$. (e) Value of the weight function $\omega(t)$ along the orbit with different ρ. (f), (g), (h) Projections of different orbits at $\rho = 17$, 15.5, 14.5, and 13.93, and (g) is an enlared part of (f) near the origin. Here, we show only the orbit in the positive x axis, and there exists a symmetry counterpart in the negative x axis. The total number of lattice points is 550 (a), (b) or 220 (c)–(h).

the smoothness and the stability of the fictitious evolution at the corner are severely damaged and a good many points are needed to depict the fine structure. In other regions, much fewer points could do the job. According to the special feature of the periodic orbit, the weight function $\omega(t)$ can be set as

$$|\bar{\mathbf{v}}_t| = \omega(t) = \frac{5}{6} + \frac{1}{|\boldsymbol{R}|}, \tag{20}$$

where $|R|$ is the radius of curvature and

$$\frac{1}{R} = \frac{1}{f^2}\left[\nabla f \cdot f - \frac{1}{2} f_v \cdot f \cdot (\nabla f^2) \cdot f\right], \quad \text{with } f = \begin{pmatrix} \dot{x} \\ \dot{y} \\ \dot{z} \end{pmatrix}. \tag{21}$$

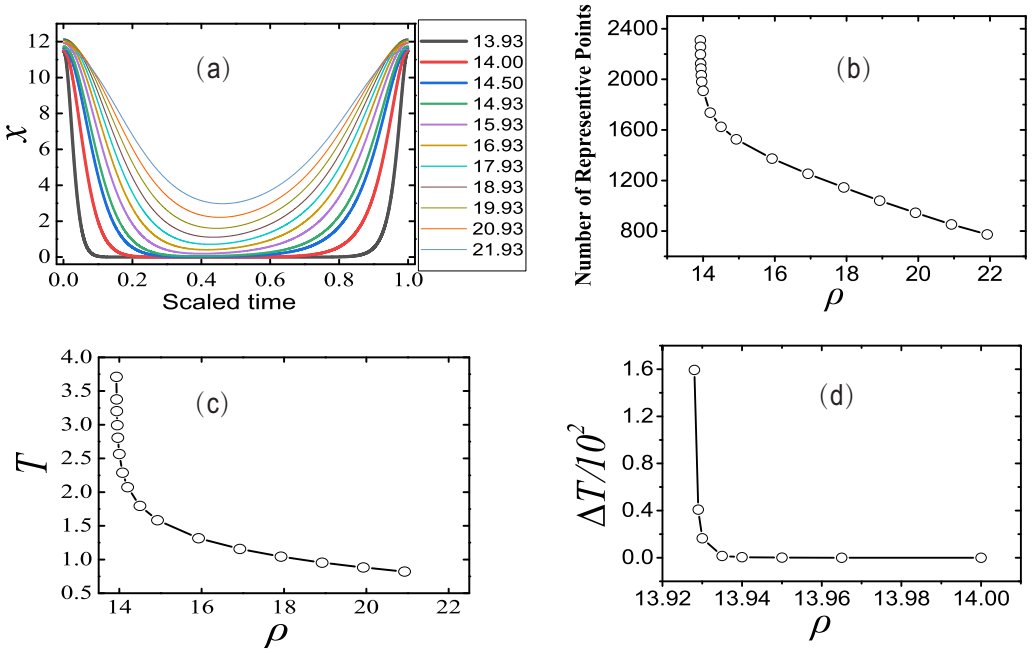

FIG. 2. (a) The x component of the periodic orbit depicted in Fig. 1 at different ρ values (distinguished by different thick lines). The abscissa is the time scaled by the period T. (b) The number N of integration points as a function of ρ. (c) The period T with the same computational accuracy as that in Fig. 1. (d) The difference of the period obtained by the Newton-Raphson method with different integration accuracy (10^{-10} vs 10^{-13}).

Equation (20) indicates that the lattice points are distributed either uniformly when this radius is large or inversely proportional to the radius when it is small. Close to the singularity, the smaller the $|R|$, the greater the density. The constant of 5/6 here marks the minimum relative density of the points, which should not be too small so as to prevent over sparsity of the lattice points along the cycle and to keep the algorithm running. In the following, $N = 220$ and $N = 550$ points are used to represent the short cycle and the long cycle, respectively, and as the gauge-fixing condition we set the y coordinates of the first point to a fixed value $y_0 = 2$.

Figure 1 displays the periodic orbits found by the modified variational method. Figures 1(a) and 1(b) first depict the projections of the long orbit (black line) and the guess loop (red line) which is obtained by Fourier transforming a close recurrence into the frequency space, keeping only the low-frequency part, and then back to the phase space at $\rho = 28$. The guess loop obviously has identical topology to the desired periodic orbit and is a very irregular orbit compared to the located periodic orbit in Fig. 1(b). As mentioned earlier, the variational method is quite robust. Despite such a bad initial condition as shown in Fig. 1(a), it still converges quite nicely to the final symmetric, butterflylike periodic orbit. Just before the onset of homoclinic explosion, the relevant periodic orbit passes closely to the fixed point located at (0,0,0), as shown in Figs. 1(c) and 1(d) at $\rho = 13.93$. The segment of the cycle in the neighborhood of the origin bends a lot, resulting in a very small radius of curvature. Figure 1(e) plots the weight function along the orbit at $\rho = 17$ (pale yellow line), 15.5 (orange line), 14.5 (line), 14 (green line), and 13.93 (black line). The outer black curve corresponds to $\rho = 13.93$, where the density of points sitting in the sharp bending area is about 4 times greater than that in other regions. With the increase of ρ, the density variation becomes smaller and almost vanishes for $\rho = 17$. Figures 1(f)–1(h) show the projections of the orbit at $\rho = 16.5$, 15.5, 14.5, and 13.93, and Fig. 1(g) is one magnified part of Fig. 1(f) near the origin where the bending corner gradually pops out with the decrease of ρ. This orbit will become a homoclinic orbit at the critical value $\rho = 13.932\,656$. However, other parts of the orbit do not change much, as shown in Figs. 1(e)–1(h), so that as ρ increases, the nonuniformity near the origin gradually builds up and more and more points are automatically allocated to this segment.

Alternatively, we may compute the short periodic orbit in Fig. 1 with the well-known Newton-Raphson method combined with the Runge-Kutta integrator with variable step size (the computational accuracy is 10^{-10}), and the results are shown in Fig. 2. On one hand, we found that a large number of representative points dwell around the fixed point (the origin) and the integrator seems to make tiny steps there, especially when the parameter ρ approaches the critical value 13.926 56 [see Fig. 2(a)], which also makes the number of integration points as well as the period T increase dramatically [see Figs. 2(b) and 2(c)]. On the other hand, we found that the result of the Newton-Raphson method starts to become inaccurate when the parameter ρ is less than 13.93, which is attributed to the fact that the Jacobian matrix J required in the Newton-Raphson method appears bizarre (namely, the values of some matrix elements are huge) as the orbit closely passes the fixed point. As a result, the calculation error is sharply increased. Shown in Fig. 2(d) is the difference in the period T obtained by the Newton-Raphson method, with different integration accuracy (10^{-10} vs 10^{-13}). It is less than 10^{-6} when ρ is greater than 13.95 but rapidly increases with ρ approaching the critical value. In the varitional approach, due to the coordinate change implemented by the automatic lattice

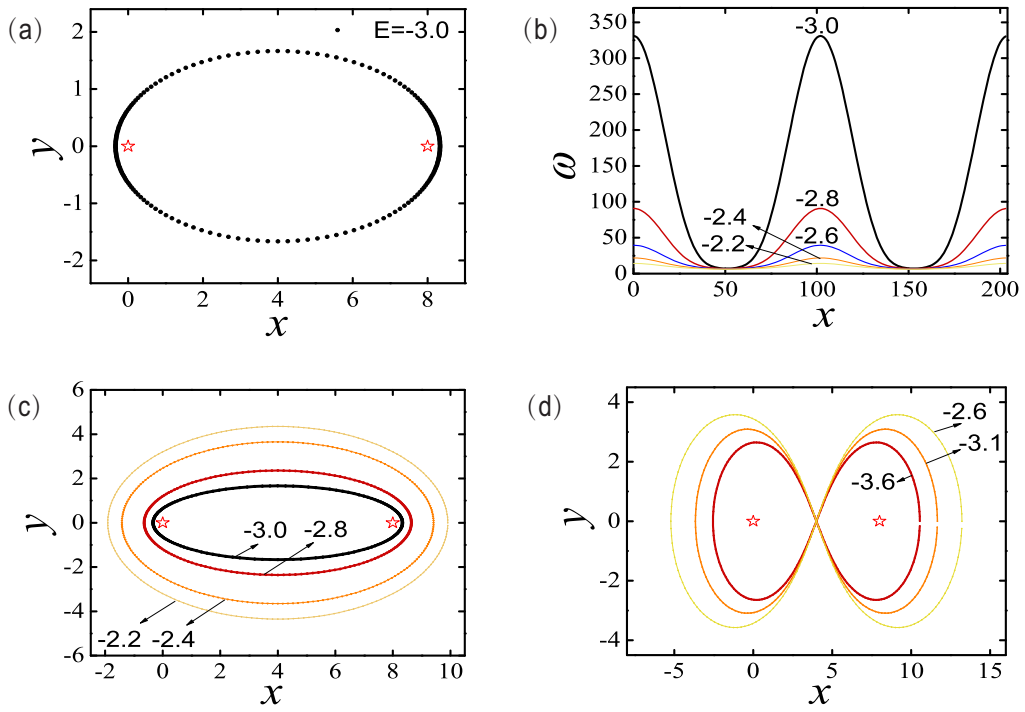

FIG. 3. (a) Distribution of points along a periodic orbit with $E = -3.0$; the weight function $\omega(t)$ (b) and one oval periodic orbit (c) at $E = -3.0, -2.8, -2.6, -2.4, -2.2$. (d) One 8-shaped periodic orbit with $E = -3.6, -3.1, -2.6$, where $R = 8$, $\epsilon = 13$, $\delta = 0.355$, $C = 0$, and $\beta = 2.4$. The y coordinate of the first point is set to a fixed value $y_0 = 0$, and the star symbol (☆) marks the positions of the fixed stars and the periodic orbit is represented by 204 points.

point allocation, this caveat is greatly reduced and for the same accuracy less than 10% of the number of points here is needed at $\rho = 13.93$, which clearly improves the efficiency.

B. Example 2

In this section, we construct a bisolar model to test the modified variational method in a Hamiltonian system with energy conservation which consists of one planet and two fixed stars with the same mass M, and the distance between the two fixed stars is R. The planet is running around the fixed stars in a plane, and the Hamiltonian of this system (in the Descartes coordinate system) is written as

$$\mathrm{H} = \frac{\left(p_x^2 + p_y^2\right)}{2m} - \frac{GMm}{\sqrt{x^2 + y^2}} - \frac{GMm}{\sqrt{(x-R)^2 + y^2}}, \quad (22)$$

where the two stars sit at the origin and (R,0), respectively. Here, m is the mass of the planet, and p_x, p_y are the two momentum components of the planet. G is the gravitational constant. The planet runs fast in the perigee and slowly at the apogee. If it is very close to the stars, the acceleration would be so great that a very high-order integrator is needed together with adaptive step size for a reliable computation, since a glitch near the star will result in a large deviation away from the singularity. For convenience, m is set to 1 and $\epsilon = \mathrm{GM}$, so that Eq. (22) is rewritten as

$$H = \frac{\left(p_x^2 + p_y^2\right)}{2} - \frac{\epsilon}{\sqrt{x^2 + y^2}} - \frac{\epsilon}{\sqrt{(x-R)^2 + y^2}}. \quad (23)$$

In this example, we have two singular points—the two stars where the potential energy of the planet becomes minus infinity and the speed positive infinity. Nevertheless, in the phase space the two singularities lie at infinity when the energy is finite. We can simply choose the weight function $\omega(t)$ proportional to the local phase-space speed:

$$|\bar{\mathbf{v}}_t| = \omega(t) = c + \frac{1}{\delta} \cdot \left[\left(\frac{\partial H}{\partial x}\right)^2 + \left(\frac{\partial H}{\partial y}\right)^2 + \left(\frac{\partial H}{\partial p_x}\right)^2 + \left(\frac{\partial H}{\partial p_y}\right)^2 \right]^{\frac{1}{2}}, \quad (24)$$

such that the new parameter is proportional to the trajectory length. Since the orbit becomes very sensitive to perturbations near the perigee and the accuracy of the computation worsens quickly, the weight function based on Eq. (24) naturally puts more points in a region near the perigee.

Figure 3 displays two typical orbits found by our method at $E_0 = -3.0$. One is an oval orbit and another is an 8-shaped one. Figure 3(a) shows the distribution of lattice points along the periodic orbit which cluster to the high-speed regions near the fixed stars. The density function is shown in Fig. 3(b), with the black thick curve marking the extremely uneven distribution of the lattice points with the ratio of the maximum and the minimum being nearly 40. Figure 3(b) also depicts the point density for other oval orbits plotted in Fig. 3(c) at $E_0 = -3.0, -2.8, -2.6, -2.4$, and -2.2. It is easy to see

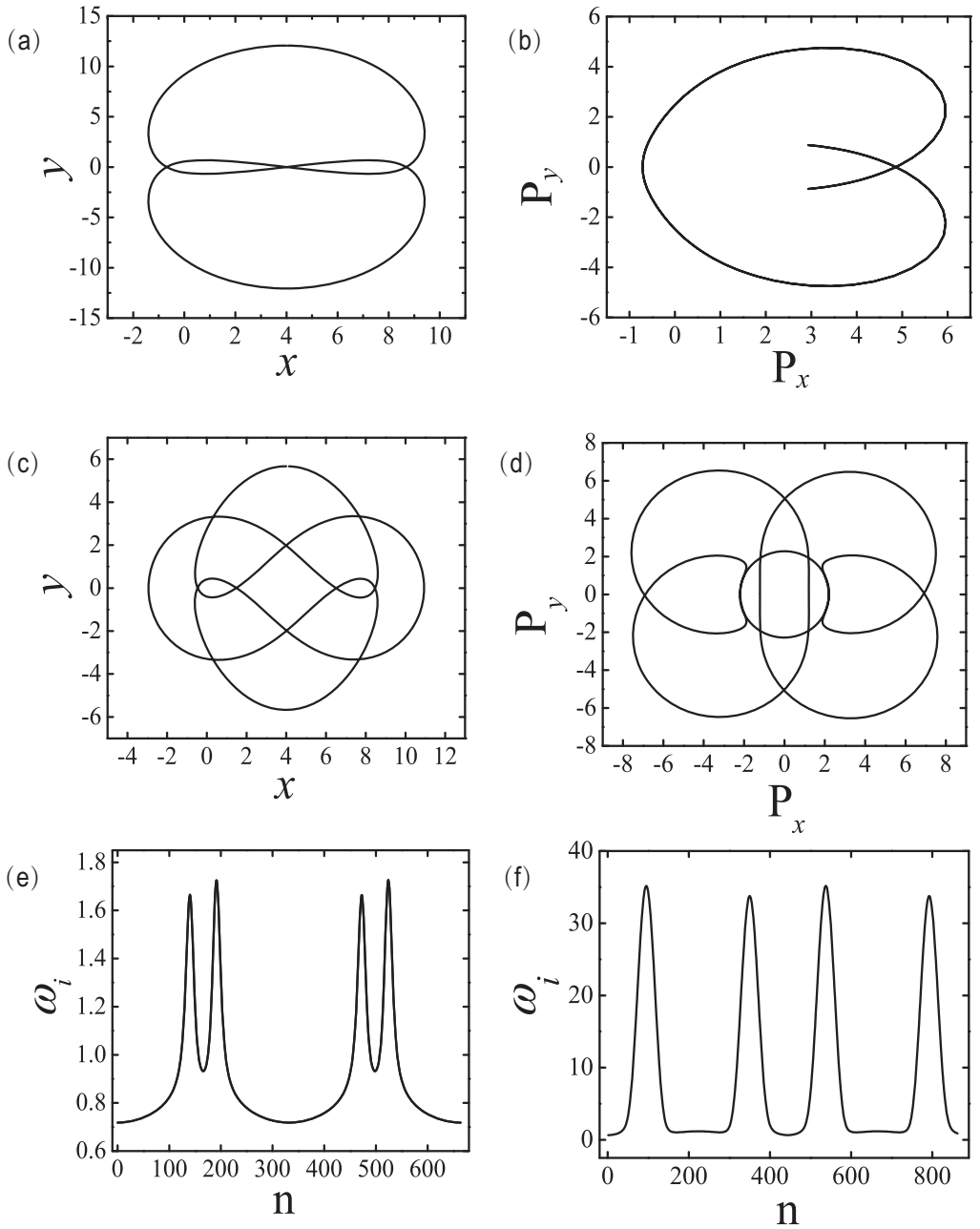

FIG. 4. Two interesting types of long periodic orbits in the bisolar model we constructed. (a), (b) The projections in the X-Y and the P_x-P_y plane of the hamburgerlike periodic orbit at $E = -1.792\,816$, $C = 0.625$, $\beta = 1.2$, $\delta = 10$, $N = 665$. (c), (d) Projections in the X-Y and the P_x-P_y plane of the Chinese-knot-like periodic orbit at $E = -3.012\,307\,9$, $C = 0.1923$, $\beta = 7$, $\delta = 2.8$, $N = 885$. (e), (f) The weight function $\omega(t)$ at $E = -1.792\,816, -3.012\,307\,9$. Other parameters are the same as in Fig. 3, and the x coordinate of the first point is set to a fixed value $x_0 = 4$.

that when the energy of an orbit is relatively high, the orbital points are basically uniformly distributed [e.g., the density function curve of the orbit with $E = -2.2$ is approximately flat, as shown in Fig. 3(b)]. With the decrease of the total energy, the orbit approaches the singularities and the density of the lattice points becomes increasingly uneven as more and more points move close to the singularities. In Fig. 3(d), we show the 8-shaped orbits at different energies. They cannot get too close to the singularities, but the weight function has the same tendency to cripple near the singularities with decreasing energy. For all the periodic orbits found by our method, the energy conservation is well preserved,

$$\Delta E = \sqrt{\sum_{i=1}^{N} (E_i - E_0)^2} \leqslant 10^{-6}, \tag{25}$$

where E_0 is the chosen value of the energy and E_i is the energy of the lattice point on the orbit. Each orbit is described by 204 lattice points.

In this model, we continue to search for period orbits with more interesting topology in order to test the practicability

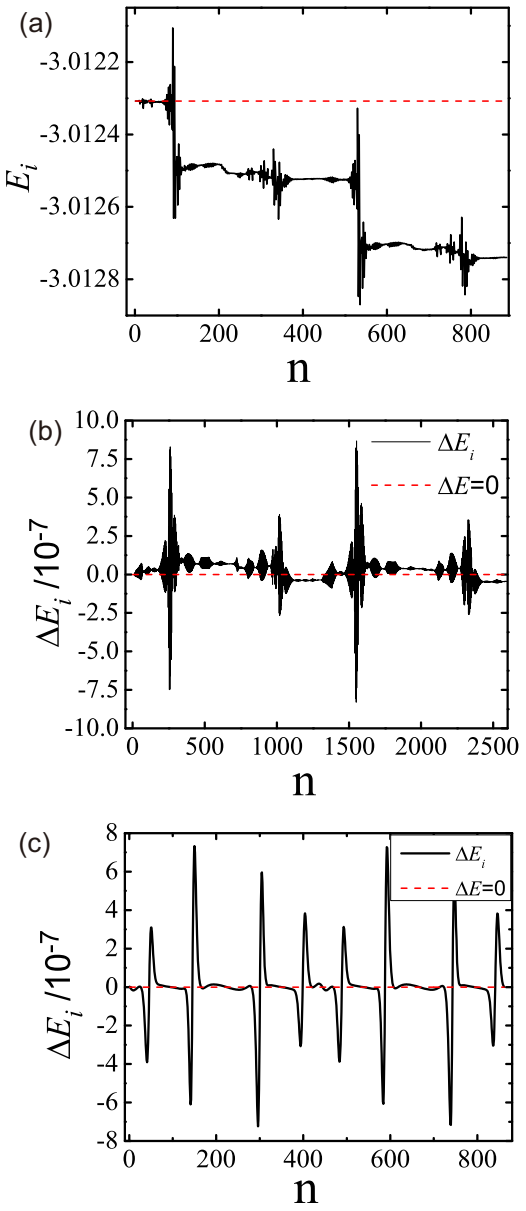

FIG. 5. (a) The energy of each point on the orbit obtained by ODE45 in MATLAB (the black solid line) and the energy (E_0) of the initial point is $-3.012\,3079$ (the dashed line), the number of representative points is 885; (b) the energy error of ODE 45 in MATLAB (the black line) for ($\Delta E_i < 10^{-6}$), and the number of representative points is 2605; (c) the energy error of our method (the black line) for ($\Delta E_i < 10^{-6}$) and the number of representative points is 885; (b), (c) the red lines indicate $\Delta E_i = 0$, where $\Delta E_i = E_i - E_0$ with $E_0 = -3.012\,307\,9$ [the corresponding periodic orbit is shown in Figs. 4(c) and 4(d)].

and stability of the variational method. Two new cycles are displayed in Fig. 4. Figures 4(a) and 4(b) depict a hamburger-like periodic orbit in the X-Y and the P_x-P_y plane. Its weight function $\omega(t)$ is shown in Fig. 4(e). Figures 4(c) and 4(d) depict a Chinese-knot-like periodic orbit, and Fig. 4(f) depicts its weight function $\omega(t)$. Whenever the orbit approaches the singularities, the density of representative points rises significantly. For the hamburgerlike cycle, the density varies

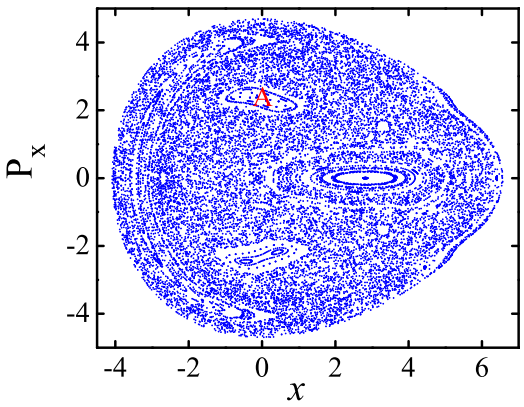

FIG. 6. The orbit structure on the Poincaré surface of section of the Hénon-Heiles system with $E_0 = 11.014$ at $y = 0.0$ and $p_y < 0$.

between 0.7 and 1.8, while for the Chinese-knot-like periodic orbit, the ratio of the maximum and the minimum density is nearly 51. Compared with the oval or 8-shaped orbits found above, they pass by the singular points in a more subtle way and are very vulnerable to perturbations or numerical instabilities. As we may see, due to this fragility whenever the orbit goes through the neighborhoods of the singularities, the total energy jitters around, which is shown in Fig. 5(a) (black solid line) such that the energy deviation between an orbit point and the initial one increases with the time lapse if no special care is taken. For the same periodic orbit [such as the one shown in Figs. 4(c) and 4(d)], if we take efforts to control the error of the energy to be less than [$10^{-6}(\Delta E_i < 10^{-6})$], similar results may be obtained by using the ODE 45 with variable step size in MATLAB, or our variational method. However, as displayed in Figs. 5(b) and 5(c), the number of representative points needed for the former is about 3 times that of the latter. Hence, the proper redistribution of lattice points may greatly reduce computation load while maintaining a reasonable accuracy.

C. Example 3

The Hamiltonian of the Hénon-Heiles system [7] is written as

$$\mathrm{H} = \frac{1}{2}\left(P_x^2 + P_y^2 + x^2 + y^2\right) + \mu x\left(y^2 - \frac{x^2}{3}\right), \qquad (26)$$

where $\mu = (0.0125)^{1/2}$. When the variational technique is applied here, the weight function has taken the same form as Eq. (24). The orbit structure on a specific Poincaré surface of section is shown in Fig. 6 for energy $E_0 = 11.014$. We can see that most areas are filled with chaotic orbits, but there still exist several resonance islands where quasiperiodic orbits lie on invariant tori which contain two noncommensurate frequencies and hence an irrational winding number. Quite many lattice points are needed to represent the whole torus in the 4-d phase space and it is awkward to describe the dynamics with these points. Nevertheless, for an invariant torus with the winding number α, it is convenient to approximate the torus with a series of periodic orbits with winding numbers $\alpha_n = \frac{p_n}{q_n} \to \alpha$, as $n \to \infty$. For sufficiently large n, the approximation is as good as one desires. However, the long

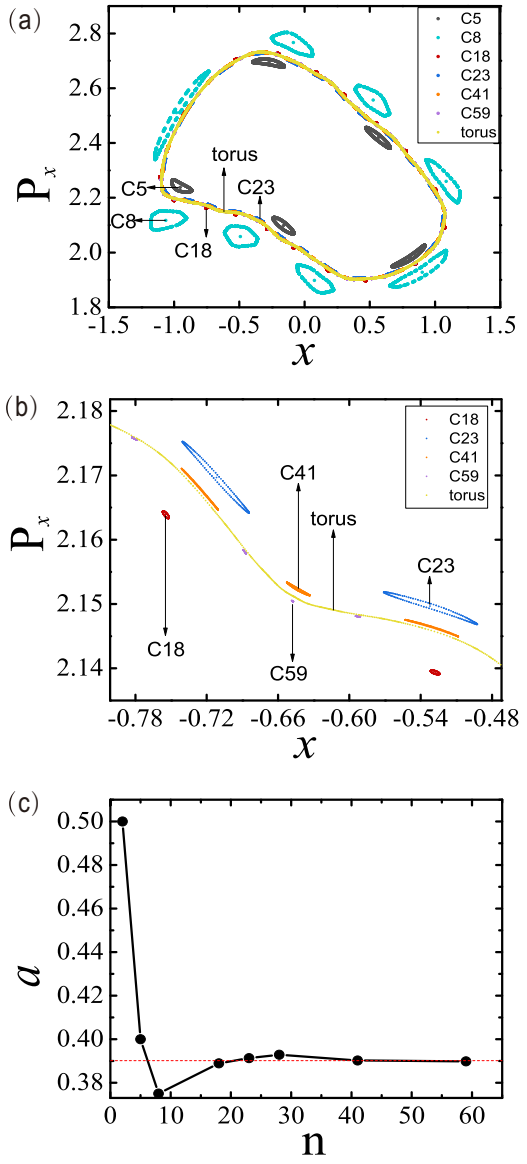

FIG. 7. (a) The periodic orbits of increasing length approaching the invariant torus marked by the yellow line; (b) magnification of part of (a); (c) the values of α_n (black dot) for the periodic orbits, with the dashed line denoting the irrational winding number of the invariant torus $\alpha = 0.390\,086\,206\,896\,552$.

period and the dynamics subtlety near the invariant torus may pose considerable difficulty to the search of these cycles. In the following, we focus on the island marked with the letter "A" in Fig. 6 and try to locate this series of periodic orbits with the current variational method. The result is depicted in Fig. 7. As shown in Fig. 7(a), the cycles approach the invariant torus (marked by the arrow) gradually, and the greater the period, the closer the cycle to the torus. Correspondingly, the winding numbers α_n of the periodic orbits also approach those of the torus as shown in (c). The convergence seems to be exponentially fast. A more detailed observation is displayed in Fig. 7(b), which is a magnification of some part of (a). As we can see, the orbits with period 41 or 59 seem to already overlap with the torus line for the plotting accuracy. Therefore the current variational approach seems good at handling this class of problems.

V. SUMMARY AND DISCUSSION

We further optimize the variational approach for searching periodic orbits proposed in Ref. [10]. Improvements are made in several aspects: First, a new equation is derived to automatically adjust the spacing between lattice points but still guarantees the exponential convergence, which bestows extra robustness and hence makes the cycle search more efficient by increasing the number of points near singularities while reducing point population in the smooth parts. Second, based on the special matrix structure in the evolution equation the LU decomposition is optimized such that the computation load is proportional to the cycle length instead of its square, and the memory consumption of the L and U matrix storage is much reduced, which gives another reduction of the computational and memory requirements for searching long periodic orbits. Finally, for conservative systems, one scheme is designed to remove the ill conditioning in the fictitious time evolution associated with the energy conservation by constructing a new velocity field which brings all orbit to the desired surface on which the dynamics remains the same as before.

The variational approach puts a guess loop near a true periodic orbit and requires an accurate enough representation with sufficiently many lattice points. In a complex system with high-dimensional phase space, the storage of these many points could be the bottleneck of the algorithm. The automatic distribution adjustment of the lattice points relieves part of the problem, especially for a cycle near a singularity. However, the computation of the Jacobian in high-dimensional systems is also time and resource consuming. How to overcome this difficulty is a major challenge for a future investigation. On the other hand, the computation of the weight function seems quite cumbersome. There may exist an equivalent way for redistributing the lattice point but with much lighter computation load. We believe that the improvement made here expands considerably the possible application scope of the variational approach, especially in the atomic and molecular physics and celestial mechanics where singular potentials routinely appear.

ACKNOWLEDGMENTS

We would like to thank Houchen Li for the Optimization of the LU decomposition. This work was supported by the National Natural Science Foundation of China under Grants No. 11375093 and No. 21473115.

[1] M. Gutzwiller, *Chaos in Classical and Quantum Mechanics* (Springer, New York, 1990).

[2] E. Ott, *Chaos in Dynamical Systems* (Cambridge University Press, Cambridge, 1992).

[3] É. Charpentier and A. Lesne, *Kolmogorov's Heritage in Mathematics* (Springer, Berlin, 2007).
[4] P. Cvitanovic, Phys. Rev. Lett. **61**, 2729 (1988).
[5] R. Artuso, E. Aurell, and P. Cvitanovic, Nonlinearity **3**, 325 (1990).
[6] Y. Lan, Commun. Nonlinear Sci. Numer. Simul. **15**, 502 (2010).
[7] P. J. Wang and G. Z. Wu, Chem. Phys. Lett. **375**, 279 (2003).
[8] P. J. Wang and G. Z. Wu, Acta Phys. Sin. **54**, 3034 (2005).
[9] J. Gao and J. B. Delos, Phys. Rev. A **49**, 869 (1994).
[10] Y. Lan and P. Cvitanovic, Phys. Rev. E **69**, 016217 (2004).
[11] D. Auerbach, P. Cvitanovic, J. P. Eckmann, G. Gunaratne, and I. Procaccia, Phys. Rev. Lett. **58**, 2387 (1987).
[12] S. C. Farantos, J. Mol. Struct.: THEOCHEM **341**, 91 (1995).
[13] J. H. B. Deane and L. Marsh, Phys. Lett. A **359**, 555 (2006).
[14] E. J. Doedel, H. B. Keller, and J. P. Kernevez, Int. J. Bifurc. Chaos Appl. Sci. Eng. **1**, 745 (1991).
[15] M. Baranger, K. T. R. Davies, and J. H. Mahoney, Ann. Phys. **186**, 95 (1988).
[16] B. Mestel and I. Percival, Physica D **24**, 172 (1987).
[17] I. S. Aranson and L. Kramer, Rev. Mod. Phys. **74**, 99 (2002).
[18] G. Kawahara and S. Kida, J. Fluid Mech. **449**, 291 (2001).
[19] C. Dong and Y. Lan, Phys. Lett. A **378**, 705 (2014).
[20] X. Zhou, W. Ren, and E. Weinan, J. Chem. Phys. **128**, 104111 (2008).
[21] W. H. Press, S. A. Teukolsky, W. T. Vetterling, and B. P. Flannery, *Numerical Recipes in C: The Art of Scientific Computing*, 2nd ed. (Cambridge University Press, Cambridge, UK, 1992).
[22] D. Viswanath, Nonlinearity **16**, 1035 (2003).
[23] D. Pingel, P. Schmelcher, and F. K. Diakonos, Phys. Rev. E **64**, 026214 (2001).
[24] P. Cvitanovic and Y. Lan, in *Proceedings of the 10th International Workshop on Multiparticle Production: Correlations and Fluctuations in QCD* (World Scientific, Singapore, 2003).
[25] E. J. Doedel, Cong. Numer. **30**, 265 (1981).
[26] E. N. Lorenz, J. Atmos. Sci. **20**, 130 (1963).
[27] Y. Liu, L. Liu, and T. Tang, J. Comput. Phys. **111**, 373 (1994).